Manganese spin dephasing mechanisms in ferromagnetic (Ga,Mn)As

I. V. Krainov,[1,2,*] V. F. Sapega,[1,†] N. S. Averkiev,[1] G. S. Dimitriev,[1] K. H. Ploog,[3] and E. Lähderanta[2]
[1]*Ioffe Physical-Technical Institute of the Russian Academy of Sciences, 194021 St. Petersburg, Russia*
[2]*Lappeenranta University of Technology, P.O. Box 20, FI-53851, Lappeenranta, Finland*
[3]*Paul-Drude-Institut fër Festkörperelektronik, Hausvogteiplats 5-7, D-10117 Berlin, Germany*
(Received 6 April 2015; revised manuscript received 5 November 2015; published 1 December 2015)

We report on the study of Mn transversal spin relaxation mechanisms in ferromagnetic (Ga,Mn)As. The spins of valence band holes experience exchange interactions with ferromagnetically ordered Mn spins and strong spin relaxation due to spin-orbit coupling. The hole subsystem provides a relaxation channel for the Mn spin subsystem. The Mn spin relaxation mechanisms were studied by means of spin flip Raman scattering. Two contributions to the spin flip Raman linewidth were found. The first one dominates below the Curie temperature and is related to the fast hole spin relaxation that damps the collective motion of the coupled Mn and hole spin subsystems. The other contribution to the Mn spin relaxation is related to spin fluctuations of the hole ensemble, which grow with temperature and become most important in the paramagnetic phase.

DOI: 10.1103/PhysRevB.92.245201 PACS number(s): 75.50.Pp, 75.78.−n, 76.20.+q, 78.30.Fs

I. INTRODUCTION

In the last two decades the diluted magnetic semiconductor (Ga,Mn)As has attracted significant attention in the scientific community, both from a fundamental point of view and as a potential candidate for spintronic device applications [1]. Although it is well established that the ferromagnetic ordering of Mn ions in (Ga,Mn)As is induced by holes, important aspects of their coupling with Mn ions in the strongly correlated hole-Mn spin system are still not fully understood. Among the open questions are the spin relaxation mechanisms of the Mn spin subsystem and the hole spin diffusion rate. Extensive studies of the collective hole-Mn ion spin excitations in (Ga,Mn)As film have been carried out by various experimental techniques, such as ultrafast magneto-optical Kerr effect [2–4] (MOKE), ferromagnetic resonance (FMR) [5,6], and picosecond strain pulses [7]. The spin dynamics in ferromagnetic (Ga,Mn)As has been studied by means of FMR, and the effective g_{eff} factor characterizing the coupled hole-Mn ion spin system has been measured as [8] $g_{\text{eff}} = 1.92 \pm 0.04$ and [9] $g_{\text{eff}} = 1.91$. The measured g_{eff} values are in good agreement with theoretical prediction—$g_{\text{eff}} = 1.90$ [10]. From the analysis of the MOKE data [11–13] the manganese transversal spin relaxation time has been estimated to be $\tau_{\text{Mn}} \sim 300 \div 400$ ps. The nonequilibrium hole spin dynamics in ferromagnetic (Ga,Mn)As has been recently studied by means of ultrafast MOKE spectroscopy, and the hole spin lifetime has been measured as [14] $\tau_h \sim 0.2$ ps. Another important ingredient of the physics of ferromagnetic (Ga,Mn)As is the hole spin diffusion rate. Despite extensive studies in this ferromagnetic semiconductor, the hole spin diffusion rate has not yet been determined. However, on the basis of the data obtained recently for electron spin diffusivity [15] $D \sim 10 \div 40$ cm^2/s in n-GaAs, one can conclude that hole spin diffusivity in (Ga,Mn)As cannot exceed this value. This conclusion is supported by the result obtained in Ref. [16] for hole transport mean-free path in (Ga,Mn)As $l_t \sim 1$ nm.

In this paper we present a direct study of the Mn transversal spin relaxation time and its g-factor renormalization in ferromagnetic (Ga,Mn)As in a wide temperature range by means of spin-flip Raman scattering (SFRS). It has been demonstrated that SFRS is an effective tool for investigating the exchange interaction and direct measurements of exchange constants in DMS based on II–VI compounds [17–19]. This technique has been successfully used to study the exchange-induced spin splitting of bound as well as free carriers in Mn-doped GaAs [20] and (Ga,Mn)As DMS [21]. In this technique the Raman shift of the SFRS line provides information on the Mn ion g factor modified by exchange interaction with valence band holes of GaAs, while the width of the SFRS line is directly related to the transversal spin relaxation time of Mn ions. The Mn g factor decreases by about 5% from its value in the paramagnetic phase ($g = 2.01$), while the SFRS linewidth, which is almost temperature insensitive below T_C, shows a strong linear increase with temperature above T_C. The study of the effect of phase (paramagnetic to ferromagnetic) transition on SFRS linewidth and its energy shift allowed us to distinguish the manganese spin dephasing mechanisms. An analytical model based on coupled manganese and hole spin subsystems, and also including fluctuations in these subsystems, is developed. This model well describes the g-factor modification and manganese spin lifetime in (Ga,Mn)As in the whole temperature range covering the ferromagnetic and paramagnetic state. Furthermore the value of hole spin diffusion coefficient is estimated by a fit of the experimental data in the frame of the developed model.

II. SAMPLES AND EXPERIMENTAL SET-UP

The 500-nm-thick (Ga,Mn)As films for this study were grown at 250°C by molecular beam epitaxy (MBE) on semi-insulating GaAs (001) substrates covered with 100 nm GaAs buffer layers. Two of the studied samples have a Mn content of $x = 0.01$ (FM1) and $x = 0.043$ (FM2). In addition, a Mn-doped (3×10^{17} cm^{-3}) 1000-nm-thick GaAs film grown

*igor.kraynov@mail.ru
†sapega.dnm@mail.ioffe.ru

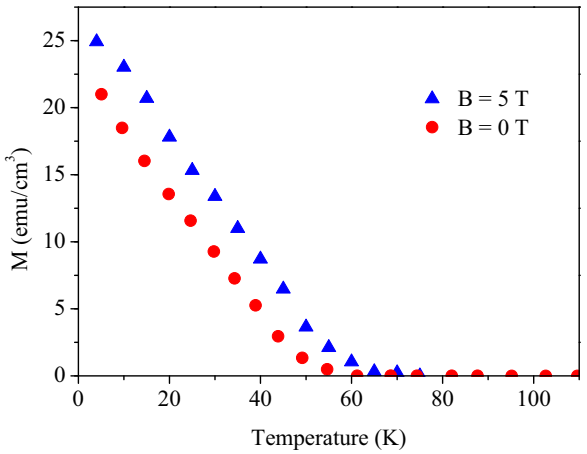

FIG. 1. (Color online) Temperature dependence of the magnetization for $Ga_{1-x}Mn_xAs$ with $x = 4.3\%$ in a magnetic field $B = 0$ T (red circles) and $B = 5$ T (blue triangles).

at 540°C was used as reference sample R. All samples studied were not subjected to annealing. Superconducting-quantum-interference-device (SQUID) measurements were carried out in the temperature range $5 \div 400$ K to investigate the macroscopic magnetic properties of the sample and to confirm the absence of MnAs nanoclusters. The SQUID measurements showed ferromagnetic (FM) behavior of samples FM1 and FM2 with Curie temperatures $T_C = 35$ K and 55 K, and saturation magnetizations $M_S = 5\,\text{emu/cm}^3$ and $M_S = 21\,\text{emu/cm}^3$, respectively. Figure 1 shows the temperature dependence of the magnetization for the FM2 sample measured in zero ($B = 0$) magnetic field (red symbols) and $B = 5$ T (blue symbols).

For the excitation of SFRS, we used the lines of He-Ne, Kr, and Ar-ion lasers. The laser power densities focused on the sample ranged from 5 to 50 Wcm^{-2}. The experiments in the temperature range $1.7 \div 200$ K were carried out in a continuous He-flow cryostat using magnetic fields up to 5 T in either the backscattering tilted Faraday or the Voigt geometry.

To describe the polarization properties of the SFRS line in the Faraday configuration we use the notation $x(\sigma^\eta,\sigma^\lambda)\bar{x}$ with $\bar{x}$ and x being perpendicular to the sample plane yz and $\eta = \pm$, $\lambda = \pm$ denoting the circular polarization of the exciting σ^η and scattered σ^λ light. The Voigt geometry corresponds to the notation $x(\sigma,\pi)\bar{x}$, with $\bar{x}$ and x perpendicular to the sample plane and the magnetic field B directed along z and σ, π denoting linear polarizations of the exciting (σ) and scattered (π) light with the electric field vector of the light perpendicular (for σ) or parallel (for π) to B.

III. EXPERIMENTAL RESULTS

In a magnetic field applied in the Voigt geometry, the Raman spectra of the FM samples as well as the R sample show a strongly polarized Mn-SFRS line with a magnetic-field-dependent Raman shift. This line is detected only in the Raman spectra measured in the $x(\sigma,\pi)\bar{x}$ Voigt configuration. In contrast, this line is absent in the exact Faraday geometry (the incident laser light and magnetic field perpendicular to the sample plane). However, tilting the incident beam by 10–15 degrees from the normal to the sample plane activates the

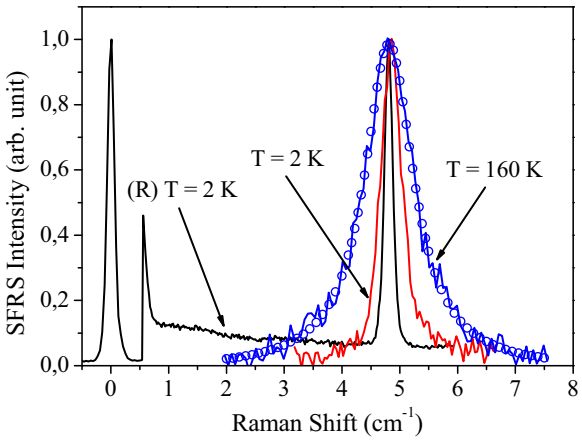

FIG. 2. (Color online) Spin flip Raman scattering spectra measured in samples with a concentration of manganese $n = 3 \times 10^{17}$ cm^{-3} (black curve) and the atomic fraction of manganese $x = 4.3\%$ (red and blue curves). The measurements were carried out in an external magnetic field $B = 5$ T and in Voigt geometry. The measurements corresponding to the black and red curves are performed at $T = 2$ K, while the blue spectrum is obtained at $T = 160$ K. The blue open circles show a Lorentzian fit.

Mn-SFRS line in crossed $x(\sigma^+,\sigma^-)\bar{x}$ polarizations. Figure 2 shows the Raman spectra for the two samples measured in the Voigt $x(\sigma,\pi)\bar{x}$ geometry at $B = 5$ T. The blue open circles represent a Lorentzian fit which is described by Eq. (4). The magnetic field dependence of the Raman shift of the Mn-SFRS line for both magnetic field geometries and $T = 2$ K is shown in Fig. 3 for the FM2 sample. For a vanishing magnetic field the Raman shift of the Mn-SFRS line of the R sample tends to zero in the Voigt and Faraday geometries and in the studied temperature range $T = 1.7 \div 170$ K. The magnetic-field dependence of the Mn-SFRS line energy shift in this sample can be represented as $\Delta_R = g^0_{\text{Mn}}\mu_B B$ with $g^0_{\text{Mn}} = 2.01$, which does not depend on temperature. In contrast in the FM samples the magnetic field dependence (see Fig. 3)

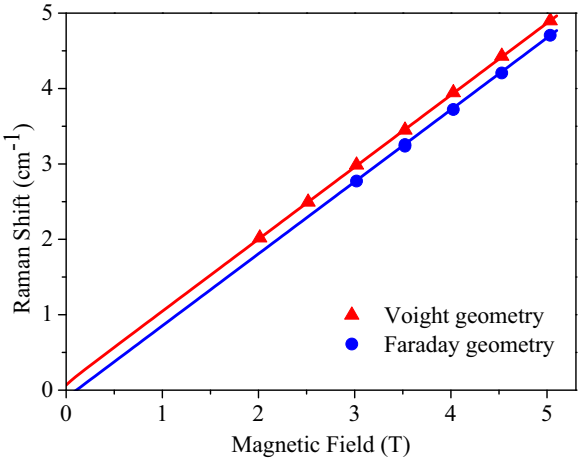

FIG. 3. (Color online) Magnetic field dependence of the SFRS Raman shift for the FM2 sample ($x = 4.3\%$) measured at $T = 2$ K in Voigt (solid red triangles) and Faraday (solid blue circles) geometries. The red and blue lines are the fits (for details see text).

of the Raman shift for the SFRS line extrapolates to a positive offset in the Voigt geometry and to a negative one in the Faraday geometry. With a temperature increase this offset decreases and vanishes at $T > T_C$. The slope (in other words, the g factor) of the magnetic field dependence of the SFRS line energy shift in the FM samples also depends on temperature. To describe the observed magnetic field dependence of the SFRS line one should take into account the magnetic anisotropy of a (Ga,Mn)As layer [22] as well as the demagnetizing field of a thin ferromagnetic layer. In the simplest approximation, the free-energy density F for a zinc-blende crystal film [such as (Ga,Mn)As] can be expressed as the sum of three contributions:

$$F = 2\pi M^2 n_x^2 - \frac{MH_2}{2} n_x^2 - \frac{MH_4}{4}\left(n_x^4 + n_y^4 + n_z^4\right), \quad (1)$$

where the first term describes the demagnetizing energy, the second and third terms are the easy plane and cubic anisotropy fields, respectively, n_i are the directional cosines, and M is the magnetization. It is assumed that the crystallographic axes coincide with the Cartesian coordinates axes x,y,z, respectively, and the x axis coincides with the growth direction of the structure. The magnetic field dependence of the Raman shift for the SFRS line in the FM samples for the Faraday and Voigt geometry can be well fitted by the following expressions:

$$\Delta_F(B,T) = g_{\text{eff}}(T)\mu_B(B - 4\pi M + H_4 + H_2), \quad (2)$$

$$\Delta_V(B,T) = g_{\text{eff}}(T)\mu_B\sqrt{(B + 4\pi M + H_4 - H_2)(B + H_4)}. \quad (3)$$

Figure 3 shows the magnetic field dependence of the SFRS line energy shift for the FM2 sample measured in the Voigt (red triangles) and Faraday (blue circles) geometries and at $T = 2$ K. The red and blue lines in this figure are the fits based on Eqs. (2) and (3). For the case of the FM2 sample the best fit was obtained with the following parameters: $H_4 = 300$ Oe, $H_2 = -1100$ Oe. Therefore, to distinguish the effect of temperature on the g factor we measured the magnetic field dependence of the SFRS line Raman shift in a wide temperature range covering the ferromagnetic and paramagnetic phases. Figure 4 shows the temperature dependence of the g factor determined as described above. The transition to the FM phase is accompanied by a decrease of Mn^{2+} ion g factor by 5%. Another important feature of the FM samples is the width of the SFRS line, which increases with temperature as shown in two spectra of Fig. 2 measured at $T = 2$ K (the red spectrum) and $T = 160$ K (the blue spectrum) and at $B = 5$ T. The temperature dependence of the SFRS linewidth measured at $B = 5$ T for the FM1 and FM2 samples is shown in Fig. 5. In each FM sample the SFRS linewidth is not sensitive to temperature below T_C and strongly increases at $T > T_C$. Typically the SFRS linewidth is determined by two factors, i.e., uniform and nonuniform lifetimes. The latter is related to the Mn g-factor dispersion. Since the SFRS linewidth in the FM samples does not depend on magnetic field, we can conclude that the measured Mn SFRS linewidth is determined exclusively by the uniform transversal lifetime of the Mn spin subsystem. Therefore the Mn spin subsystem lifetime can be determined from the SFRS linewidth. The SFRS process can be described in terms of the scattering matrix $dI/d\omega d\Omega \sim |\langle f|\hat{S}|i\rangle|^2$, where $\hat{S}$ is the scattering matrix, I is the intensity of the scattered light, and $|i\rangle$, $|f\rangle$ are the initial and final states of the photons, respectively. The third order in the perturbation gives the first nonzero contribution in the Raman line. Namely, the second order in the $\hat{V}_{ph}$ electron-photon interaction and the first order in the exchange interaction of a hole with Mn $3d^5$ electrons $\hat{V}_{ex} = A(\hat{\mathbf{S}}\hat{\mathbf{J}})$, where A is an exchange constant, and $\hat{\mathbf{S}}$, $\hat{\mathbf{J}}$ are operators of manganese spins and holes, respectively. Assuming $\hat{\mathbf{S}}^{\pm}(t) \sim e^{-\gamma t \mp i\omega_B t}$, one can show that the ratio of the Raman line's spectral density of the intensity to its maxima is as follows:

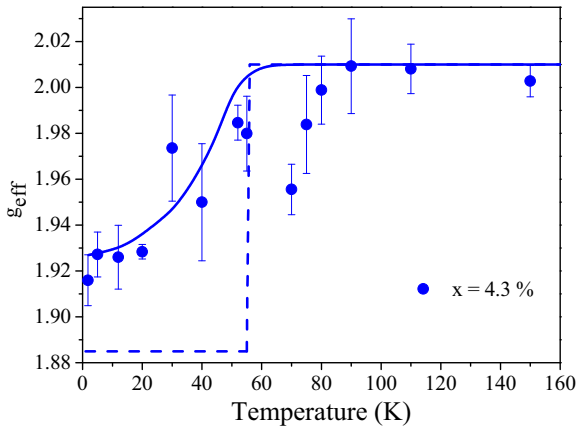

FIG. 4. (Color online) Temperature dependence of the effective Mn g factor in the FM2 $Ga_{1-x}Mn_xAs$ sample ($x = 0.043$). Dots are experimental data; solid curve is a fit based on Eq. (12). Dashed curve is a fit based on Eq. (14).

$$\frac{I_\omega(\omega)}{I_\omega(\omega_i \pm \omega_B)} \sim \frac{\gamma^2}{(\omega_i - \omega \pm \omega_B)^2 + \gamma^2}, \quad (4)$$

where I_ω is the spectral density of the intensity per unit solid angle, ω_B is the the manganese precession frequency, ω_i is the initial light frequency, and $\pm$ is the anti-Stokes and Stokes spin-flip scattering process of photoexcited holes

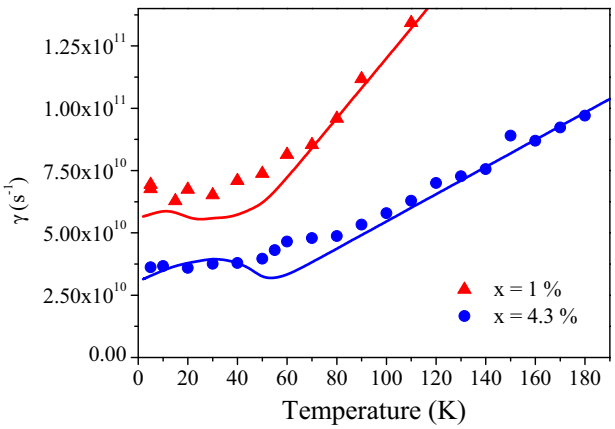

FIG. 5. (Color online) Temperature dependence of the Mn transverse spin damping frequency in $Ga_{1-x}Mn_xAs$ with $x = 1\%$ (red symbols and line) and $x = 4.3\%$ (blue symbols and line). Experiment made in Voigt geometry in a magnetic field $B = 5$ T. Solid dots and triangles are experimental data; solid curves are fits based on Eq. (13).

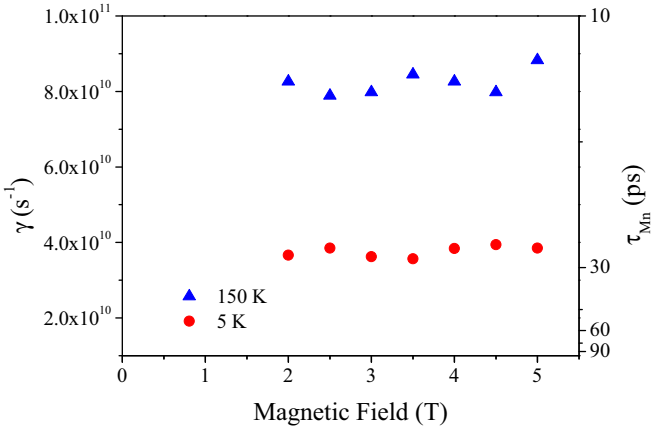

FIG. 6. (Color online) Magnetic field dependence of the Mn transverse spin damping frequency in $Ga_{1-x}Mn_xAs$ with $x = 4.3\%$ for two different temperatures. Red circles and blue triangles correspond to $T = 5$ K and $T = 150$ K, respectively.

on manganese. Let us now discuss the origin of the Stokes SFRS line (Fig. 2) in the Voigt geometry. Using linearly y-polarized light propagating along the x direction, carriers in the following spin polarizations can be excited: $|c,+\frac{1}{2}\rangle|v,+\frac{3}{2}\rangle$, $|c,+\frac{1}{2}\rangle|v,-\frac{1}{2}\rangle$, $|c,-\frac{1}{2}\rangle|v,+\frac{1}{2}\rangle$, $|c,-\frac{1}{2}\rangle|v,-\frac{3}{2}\rangle$, where c,v denote conduction band electrons and valence band holes in spherical approximation, respectively. The Stokes line appears in the SFRS spectrum due to the $\hat{S}_+\hat{J}_-$ spin flip flop process. After one spin flip flop process the carrier spin states are given by $|c,+\frac{1}{2}\rangle|v,+\frac{1}{2}\rangle$, $|c,+\frac{1}{2}\rangle|v,-\frac{3}{2}\rangle$, $|c,-\frac{1}{2}\rangle|v,-\frac{1}{2}\rangle$. One can see that light scattered in the $\overline{x}$ direction has z linear polarization when carriers recombine from $|c,+\frac{1}{2}\rangle|v,+\frac{1}{2}\rangle$, $|c,-\frac{1}{2}\rangle|v,-\frac{1}{2}\rangle$ states. From Eq. (4) one can see that the width of the line is determined by γ. Figure 6 depicts the dependence of the transverse spin relaxation rate of the Mn^{2+} ion on the external magnetic field for the FM2 sample. One can see that γ does not depend on B in the range $2 \div 5$ T either below ($T = 2$ K) or above ($T = 150$ K) T_C. Note that for the doped (R) sample the SFRS linewidth is 0.19 cm^{-1} in the full studied temperature range $2 \div 200$ K. With this SFRS linewidth we estimate the transverse spin relaxation time as $\tau_{Mn} \gtrsim 100$ ps.

IV. THEORY

It has been established in many studies that ferromagnetism in (Ga,Mn)As is caused by holes (see, e.g., Ref. [23]). Holes also modify the manganese g factor and are responsible for its spin dephasing. To describe these processes we present (Ga,Mn)As as a two magnetic subsystem [24] including the core-spin Mn^{2+} subsystem (which is characterized by a g value $g_S = 2.01$ and a subsystem magnetization $\mathbf{M}_S$) and hole subsystem whose parameters are labeled g_J and $\mathbf{M}_J$. The equations of motion for both subsystems are:

$$\frac{d\mathbf{M}_S}{dt} = C_1\frac{\mu_B g_S}{\hbar}\mathbf{M}_S \times \triangle\mathbf{M}_S + C_3\frac{\mu_B g_S}{\hbar}\mathbf{M}_S \times \triangle\mathbf{M}_J + \frac{\mu_B g_S}{\hbar}\mathbf{B}\times\mathbf{M}_S - \lambda_S\mathbf{M}_J\times\mathbf{M}_S, \quad (5)$$

$$\frac{d\mathbf{M}_J}{dt} = C_2\frac{\mu_B g_J}{\hbar}\mathbf{M}_J \times \triangle\mathbf{M}_J + C_3\frac{\mu_B g_J}{\hbar}\mathbf{M}_J \times \triangle\mathbf{M}_S + \frac{\mu_B g_J}{\hbar}\mathbf{B}\times\mathbf{M}_J - \lambda_J\mathbf{M}_S\times\mathbf{M}_J + \frac{\mu_B g_J}{\hbar}\mathbf{B}_{an}\times\mathbf{M}_J + D\triangle\mathbf{M}_J - \gamma_h\left(\mathbf{M}_J - \mathbf{M}_J^0\right). \quad (6)$$

In these expressions the first two terms describe spin waves. The C_i are constants describing the spin wave energy spectrum, whose typical values in (Ga,Mn)As are in the interval [25–27] $10^{-12} \div 10^{-13}$ cm^2. The terms containing $\lambda_S = \lambda\mu_B g_S/\hbar$ and $\lambda_J = \lambda\mu_B g_J/\hbar$ describe the interaction between the magnetic subsystems. The λ in λ_S and λ_J is a molecular field constant describing the exchange interaction between the sublattices and can be estimated by using the expression $\lambda M \sim B_{\text{eff}}$, which links the sample magnetization M with the Weiss mean field B_{eff}. Taking B_{eff} measured for (Ga,Mn)As in Refs. [28] and [29] and $M = 21$ emu/cm^3, we find that λ amounts to $10^3 \div 10^4$. In Eqs. (5) and (6) we also include the hole spin diffusion (D is a spin diffusion coefficient), the hole spin damping rate (γ_h), which is caused by the strong spin-orbit interaction in the valence band of GaAs, and anisotropy field $\mathbf{B}_{an}$ caused by complex valence band structure. Furthermore, we assume that the external magnetic field in Eqs. (5) and (6) is applied in the z direction. As we discussed above, the SFRS spectrum is characterized by the Raman shift of the SFRS line, which is determined by the precession frequency of the transverse component of the Mn spin and by the SFRS linewidth, which is determined by the dephasing rate (the transverse spin relaxation time) of the Mn spin. Both these SFRS characteristics, i.e., the eigenfrequency and the damping of the transverse component of magnetization, can be obtained from Eqs. (5) and (6). Note that the exchange interaction between magnetic subsystems modifies the g factor and leads to their spin relaxation. The anisotropy field $\mathbf{B}_{an}$ contributes to the precession frequency [see Eqs. (2) and (3)]. However this modification is important for small external magnetic fields. Our data are obtained at high magnetic fields ($B \gg H_i$) when anisotropy fields contribute as a small field independent additive to the Raman line energy shift. This one can see from Fig. 3, which presents magnetic field dependence of the SFRS Raman shift. Therefore, in order to simplify our analysis of g factor and spin relaxation, we neglect hereinafter the term with anisotropy field $\mathbf{B}_{an}\times\mathbf{M}_J$ in Eq. (6).

The equations of magnetization motion are nonlinear, however, in the approximation of a small deviation from the equilibrium they can be linearized. The solution of these equations in the linear regime allows us to describe the Mn g-factor modification. However, to describe the transverse Mn spin relaxation one has to retain the nonlinear terms in Eqs. (5) and (6). The nonlinear terms lead to two effects. The first one is a nonlinear coherent dynamics, which manifests itself in a weak dependence of the resonance frequency on its amplitude (when being small) and the second harmonic generation. The second effect is related to the existence of magnetization fluctuations in the system which lead to the Mn spin dephasing. In the regime of a small deviation from the equilibrium these effects can be analyzed independently. The nonlinear terms can be taken into account by solving the equations of motion (5)

and (6) on the z components of magnetization and substituting $M^z_{S,J}$ into the equation for the $M^{\pm}_{S,J}$ components. Then we can average the equations of motion on volume by taking the magnetization in the form $\mathbf{M}_i = \mathbf{M}_i^0 + \mathbf{M}_i(t) + \delta\mathbf{M}(x,t)$, where $\mathbf{M}_i^0$ is equilibrium magnetization, $\mathbf{M}_i(t)$ is homogeneous magnetization, and $\delta\mathbf{M}(x,t)$ is magnetization fluctuations. After averaging, the equation of motion for the homogeneous magnetization takes the following form:

$$\omega M_S^+ = \left[\omega_S - \lambda_S M_J^0 + i I_1(\omega)\right] M_S^+ + \left[\lambda_S M_S^0 - i I_2(\omega)\right] M_J^+, \tag{7}$$

$$\omega M_J^+ = \left[\lambda_J M_J^0 - i I_1(\omega)\right] M_S^+ + \left[\omega_J - \lambda_J M_S^0 + i(\gamma_h + I_2(\omega))\right] M_J^+. \tag{8}$$

In Eqs. (7) and (8) we neglect the nonlinear coherent terms, assuming the regime of a small deviation from the equilibrium. The I_i are correlations of the magnetization fluctuations and can be written as

$$I_1(t) = \frac{\lambda_S^2}{2}\langle \delta M_J^-(x,0)\delta M_J^+(x,t)\rangle + \frac{\lambda_S\lambda_J}{2}\int dx'\, G(x-x',t)\langle \delta M_J^-(x',0)\delta M_S^+(x,t)\rangle, \tag{9}$$

$$I_2(t) = \frac{\lambda_S\lambda_J}{2}\langle \delta M_S^-(x,0)\delta M_J^+(x,t)\rangle + \frac{\lambda_J^2}{2}\int dx'\, G(x-x',t)\langle \delta M_S^-(x',0)\delta M_S^+(x,t)\rangle. \tag{10}$$

The angular brackets $\langle\cdot\rangle$ in Eqs. (9) and (10) denote the statistical average with an effective Hamiltonian describing the energy of fluctuations:

$$\mathcal{H}(\delta M_S,\delta M_J) = \frac{C_1}{2}\frac{\partial\delta M_S^i}{\partial x_j}\frac{\partial\delta M_S^i}{\partial x_j} + \frac{C_2}{2}\frac{\partial\delta M_J^i}{\partial x_j}\frac{\partial\delta M_J^i}{\partial x_j} + \frac{C_3}{2}\frac{\partial\delta M_S^i}{\partial x_j}\frac{\partial\delta M_J^i}{\partial x_j} + \frac{\alpha_1}{2}\delta M_S^i\delta M_S^i + \frac{\alpha_2}{2}\delta M_J^i\delta M_J^i + \lambda\delta M_S^i\delta M_J^i, \tag{11}$$

where α_1,α_2 are phenomenological parameters of the Hamiltonian. The $G(x,t)$ is a Green function of the diffusion equation with the spin diffusion coefficient D and the damping γ_h. Also we neglect in I_i the terms containing C_i due to its small contribution to the Mn spin damping frequency. This assumption is valid for the (Ga,Mn)As parameters used for the fitting of experimental data. Now we can find the eigenvalue of Eqs. (7) and (8) describing the Mn g factor and the transverse spin relaxation frequency. The solution of the equation of motion can be obtained with the following assumptions, valid for (Ga,Mn)As [23,30]: $\lambda_i M_S^0, \gamma_h \gg \mu_B g_i B/\hbar$; $D \gg C_i\mu_B g_i M_S^0/\hbar$; $M_J^0/M_S^0 \ll 1$. Then the manganese effective g factor and the transverse spin damping frequency are

$$g_{\text{eff}}(T) \approx g_S - (g_S - g_J)\frac{\lambda_S M_J^0\left(\lambda_J M_S^0 + \lambda_S M_J^0\right)}{\left(\lambda_J M_S^0 + \lambda_S M_J^0\right)^2 + \gamma_h^2}, \tag{12}$$

$$\gamma(T) \approx \frac{T\lambda_S^2}{(2\pi)^2(D\sqrt{\alpha_J C_J} + C_J\sqrt{D\gamma_h})} + \gamma_h\frac{\lambda_S M_J^0(\lambda_J M_S^0 + \lambda_S M_J^0)}{\left(\lambda_J M_S^0 + \lambda_S M_J^0\right)^2 + \gamma_h^2}, \tag{13}$$

where $\alpha_J = (\alpha_1\alpha_2 - \lambda^2)/\alpha_1$, $C_J = (C_1C_2 - C_3^2)/C_1$. For simplicity we neglect the second term in I_1, which is smaller than the first one if $C_1 \gg C_3$. Due to the significant difference in magnetization of the Mn and hole subsystem [23], we assume that the whole magnetization of the system is determined by the manganese magnetization. To calculate temperature dependencies of $g_{\text{eff}}(T)$ Eq. (12) and $\gamma(T)$ Eq. (13), we used experimental data measured for the magnetization curve in the FM2 sample presented in Fig. 1. For further simplification we assume that the value M_J^0/M_S^0 is temperature independent.

V. DISCUSSION

The temperature dependencies of the Mn g factor and the transverse spin damping frequency (γ) calculated on the basis of Eqs. (12) and (13) are shown by the solid curves in Figs. 4 and 5, respectively. In Fig. 4 the theoretical curve is compared with the g factor measured in the FM2 sample, while Fig. 5 presents the fit of the temperature dependence of the Raman linewidth (i.e., γ) measured at $B = 5$ T for the FM1 and FM2 samples. To fit the g factor and γ of the FM1 sample, we used the following parameters: $M_J/M_S = 0.08$ (Ref. [30]), $D = 0.09$ cm^2/s, and $M_S^0 = 5$ emu/cm^3. Similarly, for the FM2 sample these parameters are $M_J/M_S = 0.02$, $D = 0.19$ cm^2/s, and $M_S^0 = 21$ emu/cm^3. The other parameters $\lambda = 2650$, $C_J = 10^{-12}$ cm^2 (Ref. [26]), $g_J = -1$ (Ref. [29]), $\gamma_h = 1.1\times10^{12}$ s^{-1} (Ref. [14]), and $\alpha_J = 5000$ are the same for the FM1 and FM2 samples. We see that the general features of our experimental results are reproduced fairly well by the calculated curves.

Let us now discuss the values of the parameters required to fit the experiment. The value of λ used in this fit can be evaluated from the known p-d exchange constant J_{pd}. The link between these two constants is given by the following expression: $\lambda\mu_B^2 = J_{pd}$. The estimate of J_{pd} value is usually based on measurements of the splitting $2\Delta_{pd}$ between the $F = 1$ and $F = 2$ states of the isolated Mn acceptor. The reported values of $2\Delta_{pd}$ cover a wide range from [20,21] $2\Delta_{pd} = 4.4$ meV to [31] $2\Delta_{pd} = 10$ meV. Using these values for $2\Delta_{pd}$ and depending on the used mean value of the hole envelope wave function at the Mn acceptor, one can get a value of J_{pd} which varies from [23,30] $J_{pd} \sim 40$ meV nm^3 to $J_{pd} \sim 2$ meV nm^3. Note that the latter value is obtained from the directly (Raman scattering) measured value $2\Delta_{pd} = 4.4$ meV and with a Mn acceptor mean radius of $r \sim 1$ nm. This is the upper limit for the value of J_{pd}, because it is obtained for the hole bound to the Mn acceptor. One can expect that for delocalized holes like in (Ga,Mn)As DMS, the value of J_{pd} should be smaller. Therefore, to exclude some uncertainty in the J_{pd} estimation, we used the value

$\lambda = 2650$ obtained from the experimentally measured Weiss field [28,29]. Another parameter involved in the fit of the experiment is the hole g factor. The value of the hole g factor in ferromagnetic (Ga,Mn)As varies from [5] $g = -0.5$ (extracted from FMR data) up to [10] $g = -2.8$ (extracted from FMR and magnetization measurement). To fit the experiment we used hole g factor $g_h = -1$ reported in Ref. [29] (extracted from magnetic-field-induced photoluminescence polarization). Note, however, that the result of the fit is not very sensitive to the value of the hole g factor.

One can see from Eq. (12) that the Mn g-factor modification is associated with a coupling between the subsystems and is sensitive to the presence of a mean magnetic moment in the system, so it is dissipative above a Curie temperature. Equation (12) has the classical limit in the case of absence of the hole spin relaxation. If we put $\gamma_h \to 0$ to zero we get the standard result [8,10,32]: the effective manganese g factor is

$$g_{\text{eff}} = \frac{M_S^0 + M_J^0}{M_S^0/g_S + M_J^0/g_J}. \tag{14}$$

The temperature dependence of the g_{eff} given by Eq. (14) is plotted (dashed line) in Fig. 4. The comparison of the calculated solid and dashed curves shows that general features of the experimental temperature dependence of the $g_{\text{eff}}(T)$ are reproduced fairly well only by Eq. (12) (solid curve), which assumes a finite value of γ_h. One can see from comparison of the dashed and solid curves in Fig. 4 that taking into account the finite value of the γ_h affects the value of g_{eff}. This means that the value of the hole spin damping rate (γ_h) estimated in our study and measured directly in Ref. [14] is not much smaller than the effective Weiss field $\lambda_J M_S^0$. Note that Eq. (14) is not valid close to the Curie point, i.e., when $B \gtrsim \lambda M_S^0(T)$.

The general behavior of the Mn transverse relaxation frequency demonstrates two regimes as follows: (i) In the temperature range up to T_C the main contribution to the Mn spin damping frequency is related to the hole spin dephasing (due to the strong spin-orbit interaction in the GaAs valence band), which, however, is not induced by Mn spins. The hole spin dephasing leads to Mn spin relaxation, because the hole spin subsystem is coupled to the Mn spin subsystem. This mechanism prevails in the ferromagnetic phase, i.e., below T_C and disappears above T_C due to a decrease of the mean magnetic moment of the system. (ii) The second contribution to the Mn spin relaxation is related to the spin fluctuations of the hole ensemble, which grow with temperature. This mechanism dominates above the Curie temperature. The fit of the experimental data by the developed theoretical model shows that the contribution of both mechanisms to the Mn spin damping frequency is comparable. Analysis of Eq. (13) (see the first term) shows that the slope of the Mn spin damping above the Curie point is determined mostly by the spin diffusion coefficient. The hole spin diffusion coefficient is proportional to the spin relaxation time and the square of Fermi velocity $D \sim v_F^2/\gamma_h$. As one can see, the denominator of Eq. (13) depends on $D\gamma_h$ which increases with the increasing of manganese concentration. This explains the decrease of the spin damping slope above T_C with an increase of Mn content (see Fig. 5). Let us now discuss the temperature dependence of the parameters for the first term denominator in Eq. (13).

TABLE I. Comparison of our results obtained by means of the SFRS technique with that measured by other methods. x is the atomic fraction of Mn in $Ga_{1-x}Mn_xAs$, d the sample width, T_C the Curie temperature, and τ_{Mn}, τ_h the manganese and hole spin relaxation time. All experiments were made at low temperatures (no more than $0.1T_C$).

Paper	x (%)	d (nm)	T_C (K)	g factor	τ_{Mn} (ps)	τ_h (ps)
Ref. [8]	6.0	5.6	72	1.92		
Ref. [9]	7.0	50	142	1.90		
Ref. [11]	6.0	200	50		288	
Ref. [12]	5.0	200	60		400	
Ref. [14]	7.5	70	77			0.2
Our result	4.3	500	55	1.91	30	0.9

The parameter C_J is temperature independent. The hole spin relaxation rate does not depend on temperature in a wide range up to T_C [14]. The Fermi velocity is temperature independent due to high manganese concentration. Thus we can conclude that the term $C_J\sqrt{D\gamma_h}$ is temperature independent. We conjecture that this conclusion is also valid for the term $D\sqrt{\alpha_J C_J}$. Note, however, that there is no information about temperature dependence of the α_J. From the fit of the $\gamma(T)$ for the FM2 sample $x = 4.3\%$ (see Fig. 5), the value of D can be estimated to be $D = 0.19$ cm^2/s. This value of D is obtained for an averaged value of the known C_J which varies from [25–27] $C_J = 10^{-13}$ cm^2 to $C_J = 10^{-12}$ cm^2. Taking into account the uncertainty in C_J and γ_h, we conclude that D falls in the interval $D \sim 0.01 \div 1$ cm^2/s. The estimated value of D seems quite reasonable. As expected the hole spin diffusion in (Ga,Mn)As is less than the electron spin diffusion in bulk GaAs $D_e \sim 10 \div 40$ cm^2/s, which was directly measured in Ref. [15]. The hole spin diffusion coefficient can be estimated from the hole transport mean-free path [16] in (Ga,Mn)As $l_t \sim 1$ nm and hole spin relaxation time [14]. The estimate with these parameters gives the hole spin diffusion coefficient ($D \sim 0.05$ cm^2/s) of the same order as obtained in our model. We assume that the increasing of manganese concentration leads to an increase of hole wave function overlap and increase of hole spin diffusion as is seen from a comparison of D measured in the FM1 ($x = 1\%$) $D \sim 0.09$ cm^2/s and FM2 ($x = 4.3\%$) $D \sim 0.19$ cm^2/s samples.

Let us now compare the present data with that obtained in earlier studies (see Table I). The value of the g factor measured in FM (Ga,Mn)As samples by ferromagnetic resonance at low temperature [8] and a few temperatures [9] are in a good agreement with that presented in Fig. 4. Also it is in a good agreement with previous theoretical calculation [10]. The hole and manganese spin relaxation times obtained in the present study are comparable with those measured by MOKE for holes [14] and Mn^{2+} [11,12], respectively. The manganese spin relaxation times estimated from time resolved MOKE data presented in Refs. [13] and [33] have the same order of magnitude as those estimated in the present study. We believe that some difference in the measured transverse Mn spin relaxation time is due to the different properties of the samples caused by such growth related characteristics as hole concentration, layer thickness, etc. As it was shown in

Refs. [13] and [33], the post growth annealing can change the magnitude of the Mn spin relaxation rate.

It is also important to compare the theory of transverse spin relaxation time developed in the present paper with the phenomenological theory by Landau-Lifshitz-Gilbert (LLG). The damping of magnetization in the LLG theory is presented by the phenomenological term in the equation of magnetization precession:

$$\frac{\partial \mathbf{M}}{\partial t} \sim \frac{\alpha_G}{M}\left[\mathbf{M} \times \frac{\partial \mathbf{M}}{\partial t}\right], \tag{15}$$

where α_G is a Gilbert coefficient (damping). In the LLG formulation the spin relaxation time is proportional to the spin precession frequency $\gamma \sim \alpha_G \omega$. While such a dependence of γ on magnetic field was not observed in this study (see Fig. 6), we conclude that the description of the spin relaxation in (Ga,Mn)As in the Bloch approach is more favorable than in LLG formulation.

VI. CONCLUSION

In conclusion we have studied the magnetization precession damping and effective Mn g-factor renormalization in ferromagnetic (Ga,Mn)As diluted magnetic semiconductor by means of spin-flip Raman scattering. We have found that two different mechanisms contribute to the transverse Mn spin relaxation time. We have obtained that in ferromagnetic (Ga,Mn)As the manganese transverse spin lifetime has the order of 30 ps, and we have measured its temperature and magnetic field dependencies. The damping magnetization precession frequency also manifests itself in the decrease of Mn g factor by 5% below Curie temperature. We have found that for a phenomenological description of magnetization damping in (Ga,Mn)As, the Bloch approach is more suitable.

ACKNOWLEDGMENTS

We thank M. Moreno for the growth of the studied samples and L. Däweritz for continuous support and encouragement. We are furthermore indebted to A. P. Dmitriev for useful discussions. The partial financial support from the Russian Foundation for Basic Research Grant No. 15-52-12017 NNIO-a, Russian Ministry of Education and Science (Contract No. 14.Z50.31.0021), Dynasty Foundation, and RF President Grant No. NSh-1085.2014.2 is acknowledged.

[1] I. Žutić, J. Fabian, and S. Das Sarma, Rev. Mod. Phys. **76**, 323 (2004).
[2] A. V. Kimel, G. V. Astakhov, G. M. Schott, A. Kirilyuk, D. R. Yakovlev, G. Karczewski, W. Ossau, G. Schmidt, L. W. Molenkamp, and T. Rasing, Phys. Rev. Lett. **92**, 237203 (2004).
[3] Y. Mitsumori, A. Oiwa, T. Słupinski, H. Maruki, Y. Kashimura, F. Minami, and H. Munekata, Phys. Rev. B **69**, 033203 (2004).
[4] D. M. Wang, Y. H. Ren, X. Liu, J. K. Furdyna, M. Grimsditch, and R. Merlin, Phys. Rev. B **75**, 233308 (2007).
[5] M. Rubinstein, A. Hanbicki, P. Lubitz, M. Osofsky, J. Krebs, and B. Jonker, J. Magn. Magn. Mater. **250**, 164 (2002).
[6] J. Sinova, T. Jungwirth, X. Liu, Y. Sasaki, J. K. Furdyna, W. A. Atkinson, and A. H. MacDonald, Phys. Rev. B **69**, 085209 (2004).
[7] M. Bombeck, A. S. Salasyuk, B. A. Glavin, A. V. Scherbakov, C. Brüggemann, D. R. Yakovlev, V. F. Sapega, X. Liu, J. K. Furdyna, A. V. Akimov *et al.*, Phys. Rev. B **85**, 195324 (2012).
[8] X. Liu, W. L. Lim, M. Dobrowolska, J. K. Furdyna, and T. Wojtowicz, Phys. Rev. B **71**, 035307 (2005).
[9] K. Khazen, H. J. von Bardeleben, J. L. Cantin, L. Thevenard, L. Largeau, O. Mauguin, and A. Lemaître, Phys. Rev. B **77**, 165204 (2008).
[10] C. Śliwa and T. Dietl, Phys. Rev. B **74**, 245215 (2006).
[11] Y. Zhu, X. Zhang, T. Li, L. Chen, J. Lu, and J. Zhao, Appl. Phys. Lett. **94**, 142109 (2009).
[12] A. V. Scherbakov, A. S. Salasyuk, A. V. Akimov, X. Liu, M. Bombeck, C. Brüggemann, D. R. Yakovlev, V. F. Sapega, J. K. Furdyna, and M. Bayer, Phys. Rev. Lett. **105**, 117204 (2010).
[13] P. Němec, V. Novák, N. Tesařová, E. Rozkotová, H. Reichlová, D. Butkovičová, F. Trojánek, K. Olejník, P. Malý, R. P. Campion, B. L. Gallagher, J. Sinova, and T. Jungwirth, Nat. Commun. **4**, 1422 (2013).
[14] A. Patz, T. Li, X. Liu, J. K. Furdyna, I. E. Perakis, and J. Wang, Phys. Rev. B **91**, 155108 (2015).
[15] T. Henn, T. Kiessling, W. Ossau, L. W. Molenkamp, D. Reuter, and A. D. Wieck, Phys. Rev. B **88**, 195202 (2013).
[16] C. Rüster, T. Borzenko, C. Gould, G. Schmidt, L. W. Molenkamp, X. Liu, T. J. Wojtowicz, J. K. Furdyna, Z. G. Yu, and M. E. Flatté, Phys. Rev. Lett. **91**, 216602 (2003).
[17] A. Petrou, D. L. Peterson, S. Venugopalan, R. R. Galazka, A. K. Ramdas, and S. Rodriguez, Phys. Rev. Lett. **48**, 1036 (1982).
[18] D. L. Peterson, D. U. Bartholomew, U. Debska, A. K. Ramdas, and S. Rodriguez, Phys. Rev. B **32**, 323 (1985).
[19] A. Petrou, D. L. Peterson, S. Venugopalan, R. R. Galazka, A. K. Ramdas, and S. Rodriguez, Phys. Rev. B **27**, 3471 (1983).
[20] V. Sapega, T. Ruf, and M. Cardona, Phys. Status Solidi B **226**, 339 (2001).
[21] V. F. Sapega, M. Moreno, M. Ramsteiner, L. Däweritz, and K. Ploog, Phys. Rev. B **66**, 075217 (2002).
[22] X. Liu and J. K. Furdyna, J. Phys. Condens. Matter **18**, R245 (2006).
[23] T. Jungwirth, J. Sinova, J. Mašek, J. Kučera, and A. H. MacDonald, Rev. Mod. Phys. **78**, 809 (2006).
[24] C. Kittel, Phys. Rev. **115**, 1587 (1959).
[25] S. Haghgoo, M. Cubukcu, H. J. von Bardeleben, L. Thevenard, A. Lemaître, and C. Gourdon, Phys. Rev. B **82**, 041301 (2010).
[26] Y.-Y. Zhou, Y.-J. Cho, Z. Ge, X. Liu, M. Dobrowolska, and J. K. Furdyna, IEEE Trans. Magn. **43**, 3019 (2007).
[27] C. Bihler, W. Schoch, W. Limmer, S. T. B. Goennenwein, and M. S. Brandt, Phys. Rev. B **79**, 045205 (2009).
[28] V. Sapega, I. Kraynov, N. Sablina, G. Dimitriev, N. Averkiev, and K. Ploog, Solid State Commun. **157**, 34 (2013).
[29] V. F. Sapega, N. I. Sablina, I. E. Panaiotti, N. S. Averkiev, and K. H. Ploog, Phys. Rev. B **80**, 041202 (2009).
[30] T. Dietl, H. Ohno, and F. Matsukura, Phys. Rev. B **63**, 195205 (2001).
[31] M. Linnarsson, E. Janzén, B. Monemar, M. Kleverman, and A. Thilderkvist, Phys. Rev. B **55**, 6938 (1997).
[32] C. Kittel, Phys. Rev. **76**, 743 (1949).
[33] J. Qi, Y. Xu, A. Steigerwald, X. Liu, J. K. Furdyna, I. E. Perakis, and N. H. Tolk, Phys. Rev. B **79**, 085304 (2009).